Results in Physics 12 (2019) 652–661

Contents lists available at ScienceDirect

Results in Physics

journal homepage: www.elsevier.com/locate/rinp

Synthesis of cobalt-rich alloys with high saturation magnetization: A novel synthetic approach by hydrazine reduction method

G. Srinivas Reddy[a], Sumit Ranjan Sahu[b,c], R. Prakash[c], M. Jagannatham[b,*]

[a] Undergraduate Program-Materials, Indian Institute of Science, Bengaluru 560012, Karnataka, India
[b] Department of Metallurgical and Materials Engineering, Indian Institute of Technology Madras, Chennai 600036, Tamilnadu, India
[c] Centre for Automotive Energy Materials, International Advanced Research Centre for Powder Metallurgy and New Materials (ARCI), Chennai 600113, Tamilnadu, India

ARTICLE INFO

Keywords:
Cobalt-rich alloys
Hydrazine reduction method
Electron microscopy
Magnetic properties

ABSTRACT

Cobalt-rich alloys of various compositions ($Co_{33}Fe_{33}Ni_{33}$, $Co_{40}Fe_{40}Ni_{20}$, $Co_{50}Fe_{25}Ni_{25}$ and $Co_{60}Fe_{20}Ni_{20}$) were synthesized from their respective precursor salts using a novel hydrazine reduction method. The synthesized nanosized powders were characterized using X-ray diffraction (XRD), scanning electron microscopy (SEM), and vibrating sample magnetometer (VSM) techniques. XRD phase analysis results revealed that the $Co_{33}Fe_{33}Ni_{33}$ alloy was formed with a pure FCC phase. Whereas, $Co_{40}Fe_{40}Ni_{20}$, $Co_{50}Fe_{25}Ni_{25}$ and $Co_{60}Fe_{20}Ni_{20}$ alloys were composed of both FCC and BCC phases. The average particle size of the alloys was estimated to be in the range of 107–280 nm. The synthesized cobalt-rich alloys exhibited ferromagnetic properties at room temperature with a high saturation magnetization value up to 138 emu/g. The mixed phase $Co_{40}Fe_{40}Ni_{20}$ alloy showed higher saturation magnetization and higher coercivity as compared to the other alloy compositions. In mixed phase alloys, the dominance of the BCC phase over the FCC phase seems to has resulted in the enhancement of the saturation magnetization value. The obtained results indicate that the hydrazine reduction method was effective in synthesizing cobalt-rich alloys with excellent soft magnetic properties.

Introduction

Magnetic materials are of significant interest to the scientific community because of their potential applications in high-density data storage, radio frequency devices, magnetic sensors and medical diagnosis [1–3]. Pure Fe, Ni, and Co are the popular materials which exhibit unique and superior magnetic properties [4]. However, nanosized particles of these elements have shown better magnetic properties compared to their bulk counterparts. Transition metal binary alloys Fe-Ni, Fe-Co, and Ni-Co have been studied extensively due to their excellent magnetic properties [5–7]. On the other hand, Co-Fe-Ni ternary alloys have got much attention due to their promising soft magnetic properties, such as high saturation magnetization (M_s) and low coercivity values (H_c) [8]. Co-Fe-Ni ternary alloys are interesting soft magnetic materials that are used in making of write heads for hard disc drives and high-frequency planar inductors [9,10]. The materials with low coercivity consume lesser energy during their usage by virtue of faster magnetization of the core and thus, enabling writing information on their disks at higher speeds [11]. The magnetic properties of these Co-Fe-Ni ternary alloys can be varied by controlling the compositional ratio of Fe, Co and Ni [12]. In previous works, Co-rich and Co-Fe-Ni ternary alloys have been synthesized *via* melt route, mechanical alloying, sputtering method, and electrodeposition techniques and subsequently, their structure and magnetic properties have been studied [13–17]. The prolonged processing time and particle morphology are the major disadvantages with the existing preparation methods of these alloys. The Co-Fe-Ni ternary alloys processed through mechanical alloying reach the saturation magnetization of 144.3–159.9 emu/g and coercivity of 15–67 Oe [18]. The composition of $Co_{65}Fe_{23}Ni_{12}$ alloy with a saturation magnetic flux density of 2.1 T and low coercivity value of < 2 Oe was processed through the electrodeposition technique [8]. The most favourable soft magnetic properties are found in Co-Fe-Ni ternary alloys comprising of both BCC and FCC phases [16]. Chemical synthesis methods have an advantage over the other conventional methods as the composition and size of the alloy nanoparticles can be controlled under specific synthesis conditions, which in turn determines the magnetic properties of the alloys [5,19].

The focus of the present investigation is to systematically study the phase formation of Co-rich alloys, the evolved morphology and size and then, to evaluate their magnetic properties. In this work, $Co_{33}Fe_{33}Ni_{33}$, $Co_{40}Fe_{40}Ni_{20}$, $Co_{50}Fe_{25}Ni_{25}$ and $Co_{60}Fe_{20}Ni_{20}$ alloys have been synthesized *via* hydrazine reduction route and their structural and

* Corresponding author.
E-mail address: jaganiitmadras@gmail.com (M. Jagannatham).

https://doi.org/10.1016/j.rinp.2018.12.016
Received 29 November 2018; Accepted 4 December 2018
Available online 08 December 2018

morphological characterizations were carried out. Further, the magnetic properties of the as-synthesized alloys were evaluated. The compositions of the alloys were chosen from the phase diagram reported for Co-Fe-Ni bulk alloys [17]. Here, one of the selected compositions is from FCC phase region (equiatomic, $Co_{33}Fe_{33}Ni_{33}$) and another composition ($Co_{40}Fe_{40}Ni_{20}$) is from the mixed BCC and FCC phase region. Whereas, the other two compositions ($Co_{50}Fe_{25}Ni_{25}$ and $Co_{60}Fe_{20}Ni_{20}$) were chosen near to the boundary region of the FCC to BCC phase transformation.

Experimental details

The $Co_{33}Fe_{33}Ni_{33}$, $Co_{40}Fe_{40}Ni_{20}$, $Co_{50}Fe_{25}Ni_{25}$ and $Co_{60}Fe_{20}Ni_{20}$ alloys were synthesized using hydrazine ($N_2H_4{\cdot}H_2O$) as a reducing agent by designing a simple air exhausting device, which avoids the requirement of an inert atmosphere. A schematic sketch of the synthesis process is shown in Fig. 1. All the precursor chemicals $CoCl_2{\cdot}6H_2O$, $Ni(NO_3)_2{\cdot}6H_2O$ and $Fe(SO_4).7H_2O$ were of analytical grade and were used for the preparation of the alloys without further purification. In a typical synthesis, predetermined quantities of the precursors were dissolved in ethanol-water solution at a fixed volume ratio of 3:1 inside a conical flask. This precursor solution was stirred using a magnetic stirrer for 20 min to obtain a homogenous solution. Further, NaOH solution of 6 M was added to the above solution to obtain a pH value of 11. The resultant solution was heated to 100 °C under constant magnetic stirring. Then, 10 ml of hydrazine ($N_2H_4{\cdot}H_2O$) was slowly added into the above the precursor solution. In order to prevent the interaction of air with the reaction vessel, the reaction was carried out inside a conical flask having a side neck outlet which is connected to a rubber pipe immersed into a water bath. Gases and vapours released during the reaction were bubbled into the water. The solution was maintained at 100 °C for 45 min. The resulting black precipitate was filtered and washed several times with ethanol to remove the chloride and other contaminant ions. The final product was dried inside a vacuum oven at 60 °C for 4 h.

The phases of the as-synthesized alloys were identified using X-ray diffractometer (XRD, X'pert PROPANanlytical) with Cu K_α ($\lambda = 0.154$ nm) radiation. The morphology of the alloys and their elemental compositions were observed using a scanning electron microscope (SEM, Zeiss, Operating voltage 15 kV) equipped with an energy dispersive X-ray spectroscopy (EDS) detector. The magnetic characterization was carried out at room temperature on a Vibrating Sample Magnetometer (VSM) (Microsense, Model EV9) equipped with a 20 kOe magnetic field.

Results and discussion

The alloys with the compositions $Co_{33}Fe_{33}Ni_{33}$, $Co_{40}Fe_{40}Ni_{20}$, $Co_{50}Fe_{25}Ni_{25}$ and $Co_{60}Fe_{20}Ni_{20}$ were synthesized *via* hydrazine reduction method. The XRD patterns of the ternary alloys are shown in Fig. 2a. From the XRD patterns, it can be observed that additional impurity phases, such as cobalt oxide, iron oxide and nickel oxide are not present in the as-synthesized alloys. For the synthesized alloys, the FCC phase was characterized by the five reflections: (1 1 1), (2 0 0), (2 2 0), (1 1 3) and (2 2 2) and the BCC phase was characterized by two reflections: (1 1 0) and (1 1 2). The deconvoluted major peaks for each of the alloys are shown in Fig. 2b. The area under the FCC (1 1 1) and BCC (1 1 0) reflections were used to calculate the phase fractions of the FCC and BCC phases, respectively. The pure FCC phase was obtained for the equiatomic solid solution of composition $Co_{33}Fe_{33}Ni_{33}$ which belongs to the FCC phase region of the Co-Fe-Ni ternary phase diagram [17]. In the case of other ternary compositions, $Co_{40}Fe_{40}Ni_{20}$, $Co_{50}Fe_{25}Ni_{25}$ and $Co_{60}Fe_{20}Ni_{20}$, the XRD patterns comprise of both BCC and FCC phases. In $Co_{40}Fe_{40}Ni_{20}$ both the BCC and FCC phases have formed in significant proportions [20,21] as the composition of the alloys falls in the mixed BCC and FCC phase region of the phase diagram. Whereas, in the case of $Co_{50}Fe_{25}Ni_{25}$ and $Co_{60}Fe_{20}Ni_{20}$ alloys, the major phase is FCC, along with the minor amount of the BCC phase as these compositions correspond to the boundary region of the BCC to FCC phase transformation in the phase diagram. The formation of the minor BCC phase can be attributed to the possible effect of different reduction rates of the metal precursor salts, where one of the precursors started reducing at a slightly faster rate than the other precursors, during the alloy formation process. The formation of the minor BCC phase may also be associated with the change in the nucleation and growth rates in ternary alloys [22,23].

The phases related to the corresponding compositions and their lattice parameters are shown in Table 1.

The lattice parameter (a) of the cubic phase was calculated using the following relation:

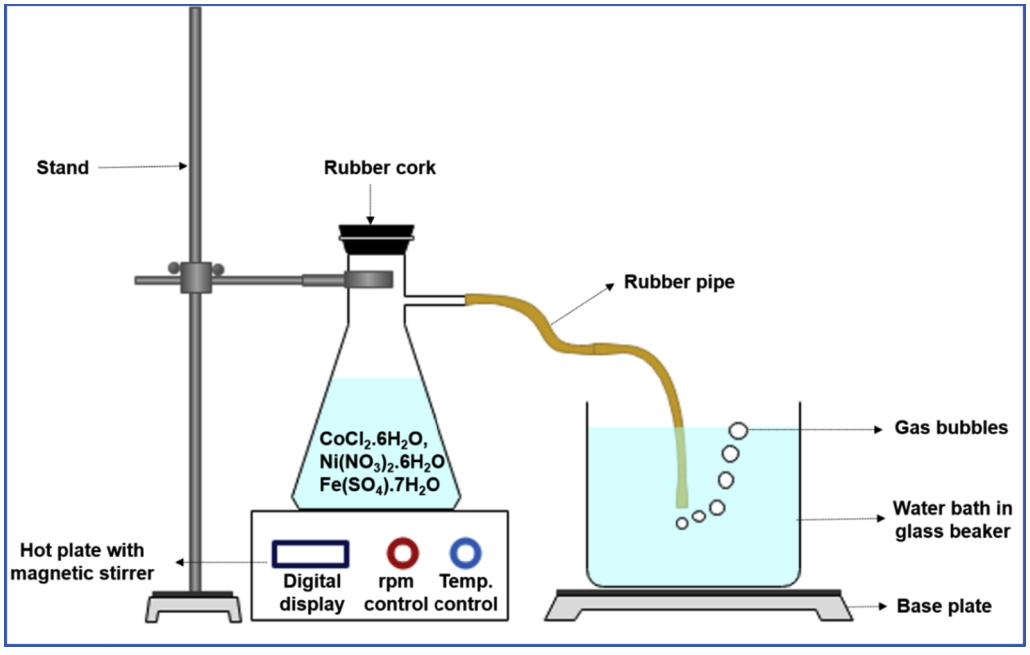

Fig. 1. Schematic sketch of the synthesis process for Co-Fe-Ni alloys *via* hydrazine reduction method.

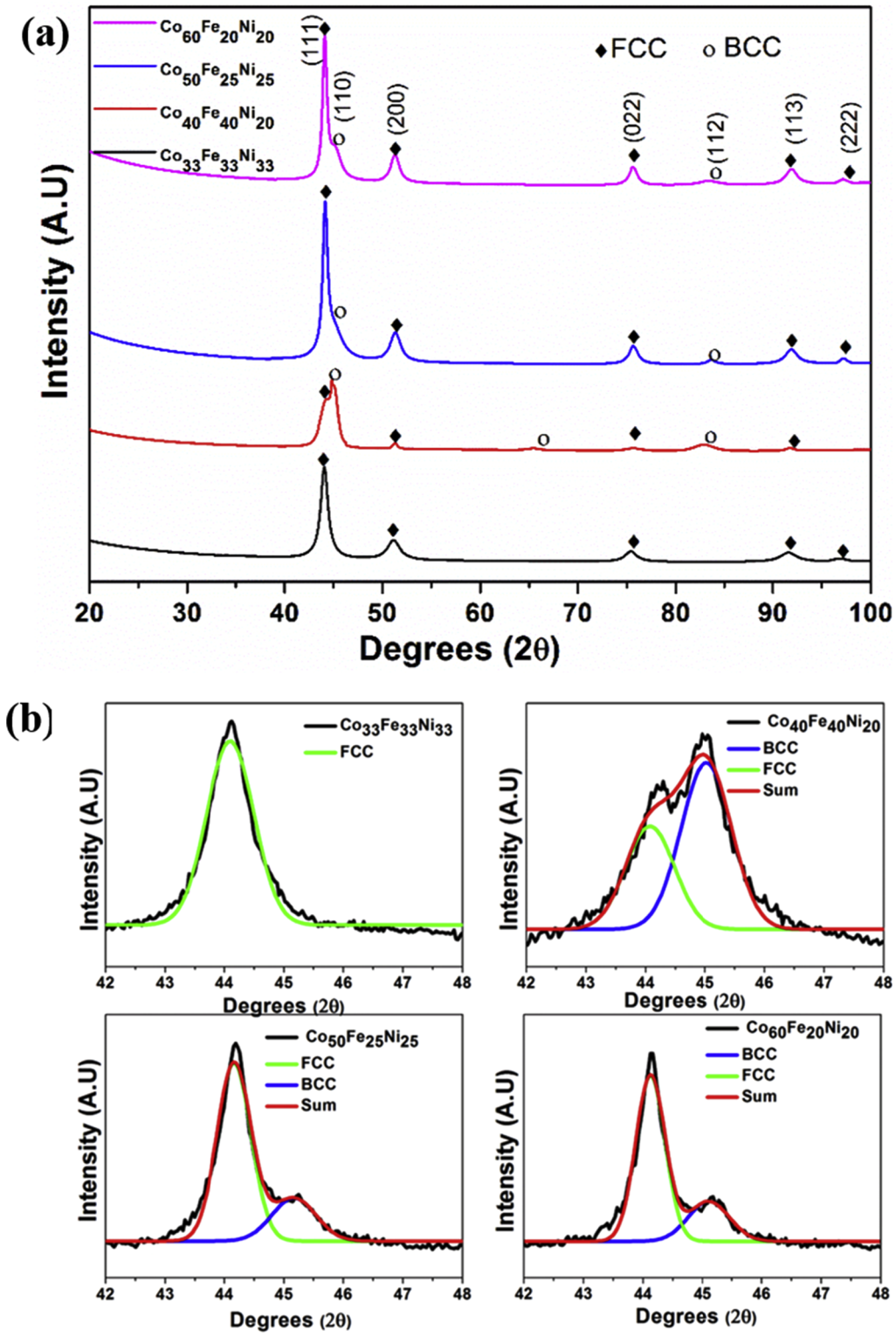

Fig. 2. (a) XRD pattern of $Co_{33}Fe_{33}Ni_{33}$, $Co_{40}Fe_{40}Ni_{20}$, $Co_{50}Fe_{25}Ni_{25}$ and $Co_{60}Fe_{20}Ni_{20}$ alloys and (b) corresponding deconvoluted XRD peaks.

$$a = \frac{\lambda(h^2 + k^2 + l^2)^{\frac{1}{2}}}{2sin\theta}$$

where h, k, l are the Miller indices of the plane of the phase, θ is the Braggs angle.

The morphology of the $Co_{33}Fe_{33}Ni_{33}$, $Co_{40}Fe_{40}Ni_{20}$, $Co_{50}Fe_{25}Ni_{25}$ and $Co_{60}Fe_{20}Ni_{20}$ alloys was investigated using SEM and the morphology of the powders are shown in Figs. 3–6 respectively. From the SEM images of the alloys, it can be clearly observed that the morphology of the particles changes with the change in the cobalt content [24]. Several factors affect the particle size and morphology of the synthesized alloys, such as solvent, crystal structure, elemental composition and reduction rate of elements [7,25]. Typically, high cobalt content in the alloy forms dendritic morphology [1,7,26]. Figs. 3 and 4 show that the $Co_{33}Fe_{33}Ni_{33}$, $Co_{40}Fe_{40}Ni_{20}$ alloys exhibit spherical morphology with uniform particle size. With the increase in the cobalt content ($Co_{50}Fe_{25}Ni_{25}$ and $Co_{60}Fe_{20}Ni_{20}$), a very low fraction of

Table 1
Structural data for the Co-Fe-Ni alloys prepared by hydrazine reduction method.

Alloy composition	Phase obtained from XRD (Phase fraction, %)	Lattice parameter (Å)
$Co_{33}Fe_{33}Ni_{33}$	FCC (100)	3.555
$Co_{40}Fe_{40}Ni_{20}$	FCC (41)	3.545
	BCC (59)	2.852
$Co_{50}Fe_{25}Ni_{25}$	FCC (70)	3.551
	BCC (30)	2.838
$Co_{60}Fe_{20}Ni_{20}$	FCC (66)	3.554
	BCC (34)	2.836

dendrites was observed along with the spherical particles (Figs. 5c, d, 6c and d). The change in the morphology with an increase in cobalt content may be attributed to the rate of the reduction process of metal precursor salts by hydrazine under present conditions [27]. Spherical morphology of the particles is formed due to the faster reduction reaction resulting in faster grain growth. This helps in the growth of various facets (isotropic growth) and forms particles with spherical morphology. The dendritic morphology is formed due to the nucleation of alloys as small nuclei. The small nuclei are unstable because of their high surface energy and high surface curvature. In order to decrease the surface energy, several small nuclei aggregate together to form a dendritic structure along a specific direction (anisotropic growth) [26,27]. The EDS pattern for the $Co_{33}Fe_{33}Ni_{33}$, $Co_{40}Fe_{40}Ni_{20}$, $Co_{50}Fe_{25}Ni_{25}$ and $Co_{60}Fe_{20}Ni_{20}$ alloys are shown in Fig. 3d, 4d, 5f and 6f respectively. The atomic percentage of the elements in the alloys were calculated from the intensity of the peaks corresponding to Co, Fe and Ni in the EDS spectra. The compositions of the alloys obtained from the EDS spectra are in good agreement with the actual synthesized compositions. These elemental analysis results clearly indicate that the metal ions were completely reduced to their metallic form by hydrazine to form Co-Fe-Ni alloys with the desired composition.

It should also be noted that the EDS spectra of the alloys contain a minor peak corresponding to oxygen. This could be due to the encapsulation of the surface of the nanoparticles with a very thin oxide layer and are not identified from XRD analysis. Similar results have also been reported in previous works [28,29].

The average size of the spherical particles was calculated from the SEM images for each of the alloy compositions. To calculate the average particle size, ~100 particles were selected and their sizes were measured using ImageJ image analyser software. The distribution and average particle sizes of all the compositions are shown in Fig. 7 which ranges from ~107 to ~280 nm. It could be observed that the average particle size of the alloys increases with increase in the cobalt content with an exception in $Co_{40}Fe_{40}Ni_{20}$ where the average particle size was found to be the smallest (~107 nm), which could be due to the competitive nucleation and growth process of BCC and FCC phases [30]. The change in particle size with change in elemental composition has also been reported in previous works [25,28].

The magnetic properties of the alloys were measured by VSM at room temperature with an applied magnetic field of -20 kOe $< H_c <$ 20 kOe. Fig. 8a shows the room temperature magnetic

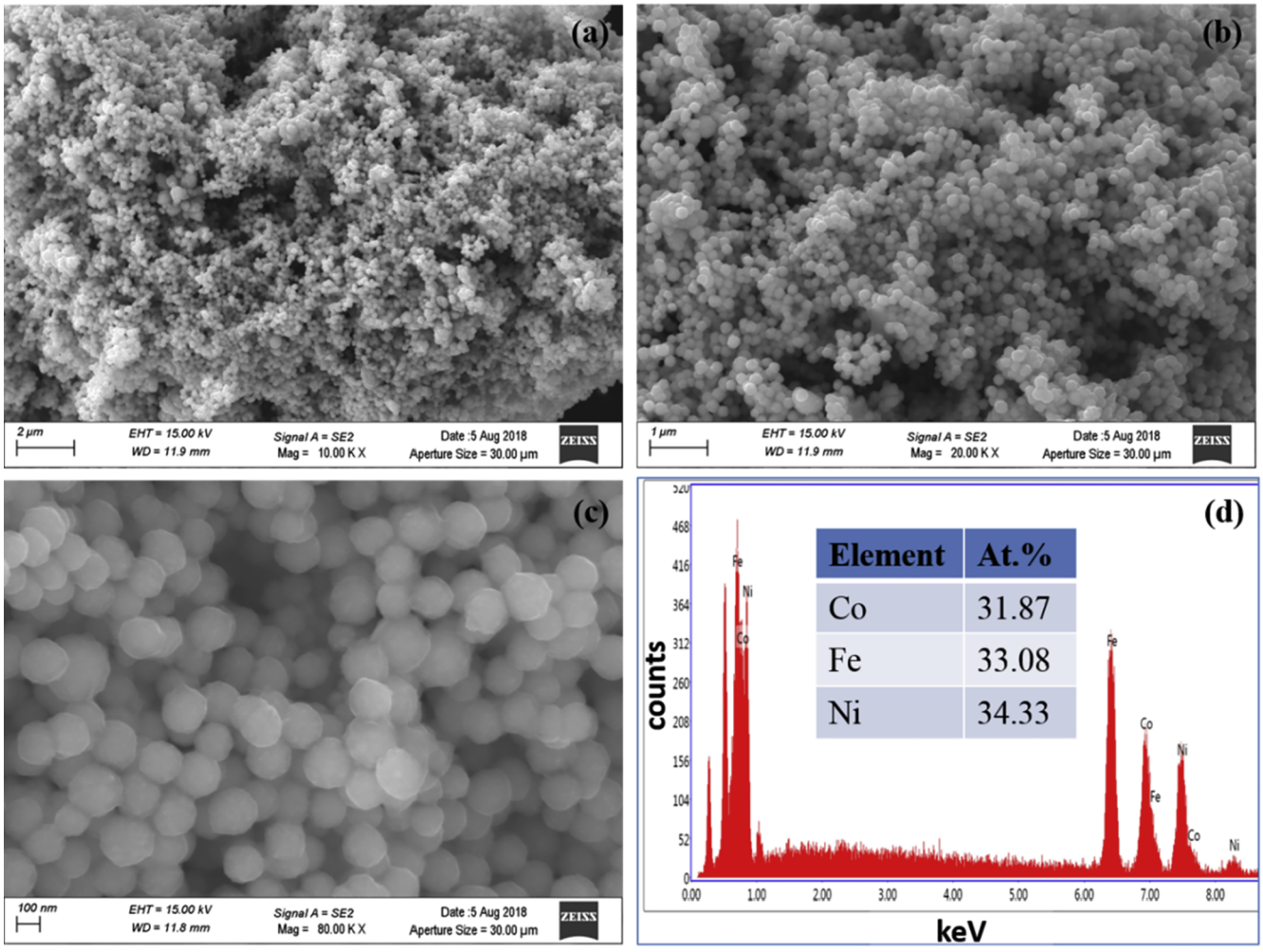

Fig. 3. (a–c) SEM images of $Co_{33}Fe_{33}Ni_{33}$ at different magnifications and (d) corresponding EDS spectrum.

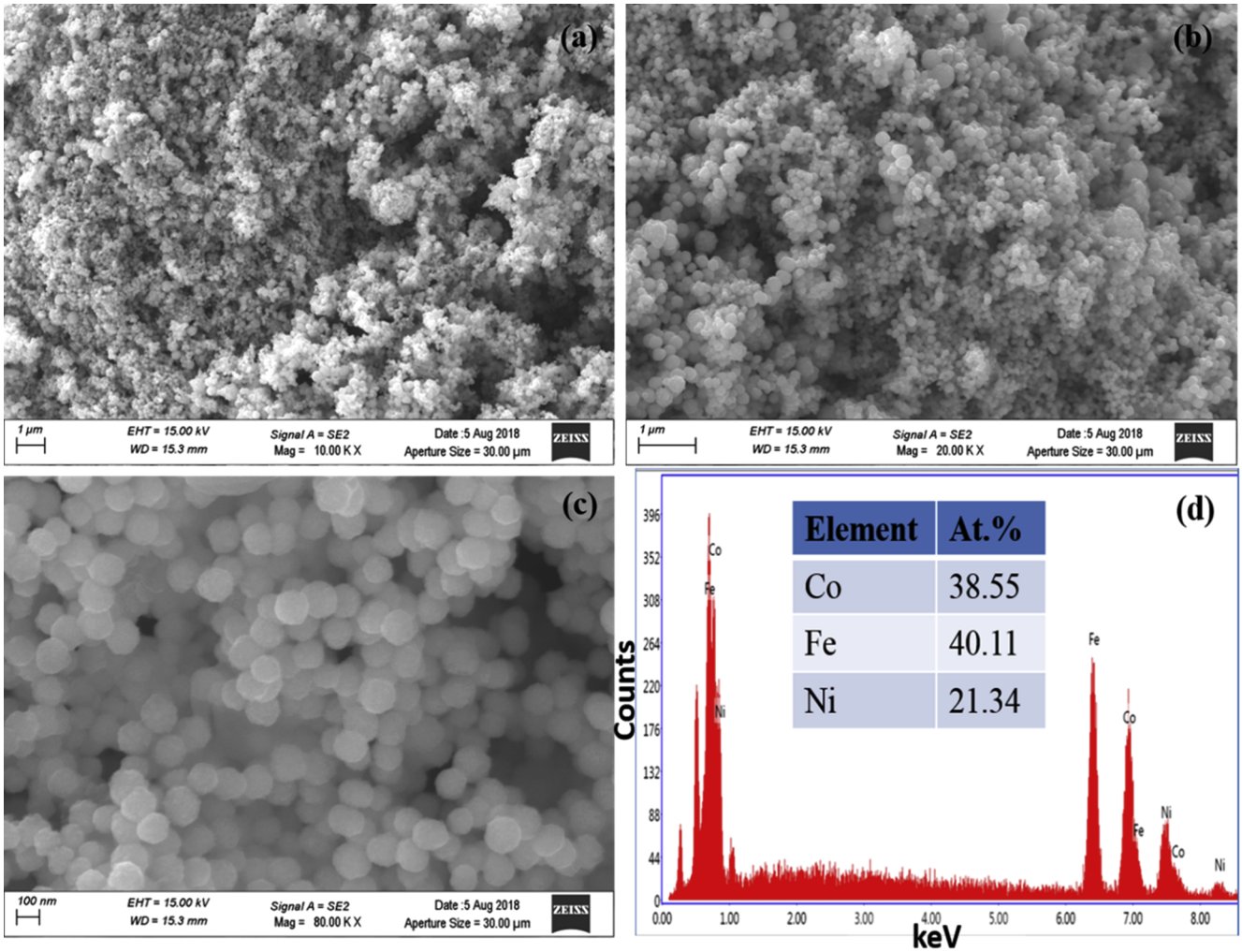

Fig. 4. (a–c) SEM images of $Co_{40}Fe_{40}Ni_{20}$ at different magnifications and (d) corresponding EDS spectrum.

hysteresis curve for the $Co_{33}Fe_{33}Ni_{33}$, $Co_{40}Fe_{40}Ni_{20}$, $Co_{50}Fe_{25}Ni_{25}$ and $Co_{60}Fe_{20}Ni_{20}$ alloys. From the hysteresis curves, it can be observed that all the synthesized compositions exhibit ferromagnetic behaviour. An enlarged view of the hysteresis curve at zero magnetic field is shown in Fig. 8b. The observed saturation magnetization (M_s) and coercivity (H_c) values are shown in Fig. 8c. The magnetic saturation of 111.6, 138.1, 131.8 and 135.4 emu/g was obtained for the $Co_{33}Fe_{33}Ni_{33}$, $Co_{40}Fe_{40}Ni_{20}$, $Co_{50}Fe_{25}Ni_{25}$ and $Co_{60}Fe_{20}Ni_{20}$ alloys respectively. Saturation magnetization and coercivity are strongly depend on the composition, particle size, surface anisotropy in different shapes and the ratio of the BCC to FCC phases [31]. On the other hand, most favourable saturation magnetization properties are found in materials having both phases [10,31–33]. The dominance of the BCC phase over the FCC phase in a two-phase alloy is beneficial for obtaining high saturation magnetization [31,34]. Among all compositions, $Co_{40}Fe_{40}Ni_{20}$ exhibited a larger value of saturation magnetization (138.1 emu/g) due to the enhancement of magnetic saturation by BCC phase [31,34]. Particle size also has a significant effect on the saturation magnetization of the alloys. Smaller particle size results in lower saturation magnetization than that of larger particle size. The low saturation magnetization for smaller particles can be explained in terms of its non-collinear spin arrangement at near the surface of the particle [35]. Therefore, the saturation magnetization increases as the size of the particle increases. An increase in the saturation magnetization was observed (111.6, 131.8 and 135.4 emu/g) for the samples $Co_{33}Fe_{33}Ni_{33}$ (186 nm), $Co_{50}Fe_{25}Ni_{25}$ (230 nm) and $Co_{60}Fe_{20}Ni_{20}$ (280 nm), respectively.

It can be noticed from the magnetic hysteresis curves that the obtained coercivity values of the alloys are relatively higher than that of the ternary alloys prepared *via* other wet chemical routes [25,28]. However, the obtained coercivity values are relatively lower than the alloys processed through the electro-deposition technique at room temperature [8]. The coercivity of all the compositions was calculated from the magnetic hysteresis loops. Several factors which affect the coercivity of nanosized particles, such as composition, surface anisotropy and shape anisotropy [31]. The coercivity values increased with the increase in the Co and Fe content or decrease in the Ni content as shown in previous reports [28,36]. Surface anisotropy is created mainly due to missing of coordinating atoms around the surface of the metal particle. Compared to other morphology, the particles with spherical morphology exhibit higher coercivity values. The enhancement of coercivity with spherical nanosized particles has also been reported earlier [37]. On the other hand, dendritic morphology of the particle exhibits shape anisotropy [38,39]. In this context, looking into the morphology of the synthesized alloys, $Co_{33}Fe_{33}Ni_{33}$ and $Co_{40}Fe_{40}Ni_{20}$ exhibit only spherical morphology. The $Co_{33}Fe_{33}Ni_{33}$ have pure FCC crystal structure and only spherical morphology. Therefore $Co_{33}Fe_{33}Ni_{33}$ exhibited lower coercivity (101 Oe) than other samples. However, the coercivity of $Co_{40}Fe_{40}Ni_{20}$ was found to be higher (162 Oe) compared to the other samples. It may be attributed to the finer particle size (107 nm) possessing a high anisotropy field than that of the larger particles which have resulted in the higher coercivity value [40]. Moreover, the higher Fe content in $Co_{40}Fe_{40}Ni_{20}$ alloy results in higher

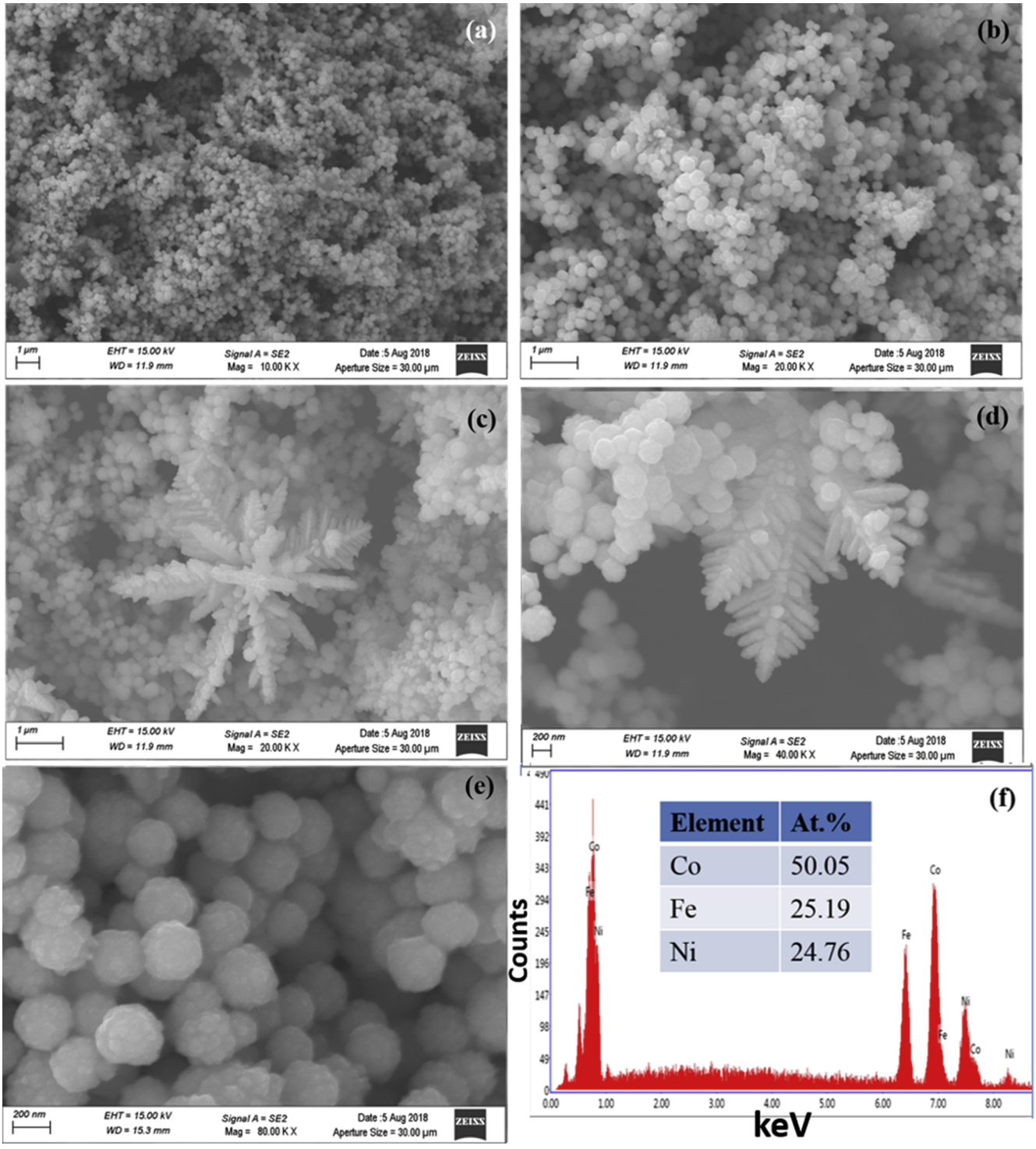

Fig. 5. (a–e) SEM images of $Co_{50}Fe_{25}Ni_{25}$ at different magnifications and (f) corresponding EDS spectrum.

coercivity. The $Co_{50}Fe_{25}Ni_{25}$ and $Co_{60}Fe_{20}Ni_{20}$ exhibit spherical particles along with a small fraction of dendritic morphology. The $Co_{60}Fe_{20}Ni_{20}$ alloys exhibit more coercivity (137 Oe) than $Co_{50}Fe_{25}Ni_{25}$ alloy (113 Oe), due to the formation of more amount of dendrite morphology (shape anisotropy), as observed in the SEM images. Overall the saturation magnetization of the synthesized alloys was high, while the coercivity values are relatively comparable to that of the previous works [28,41].

Summary and conclusions

Nanoparticles of Co-rich alloys ($Co_{33}Fe_{33}Ni_{33}$, $Co_{40}Fe_{40}Ni_{20}$, $Co_{50}Fe_{25}Ni_{25}$ and $Co_{60}Fe_{20}Ni_{20}$) were successfully synthesized *via* hydrazine reduction route. This method is very simple and fast for preparing nanosized particles of Co-rich alloys. Single FCC phase was formed in the case of equiatomic composition $Co_{33}Fe_{33}Ni_{33}$ and different fractions of BCC and FCC phases were observed in other

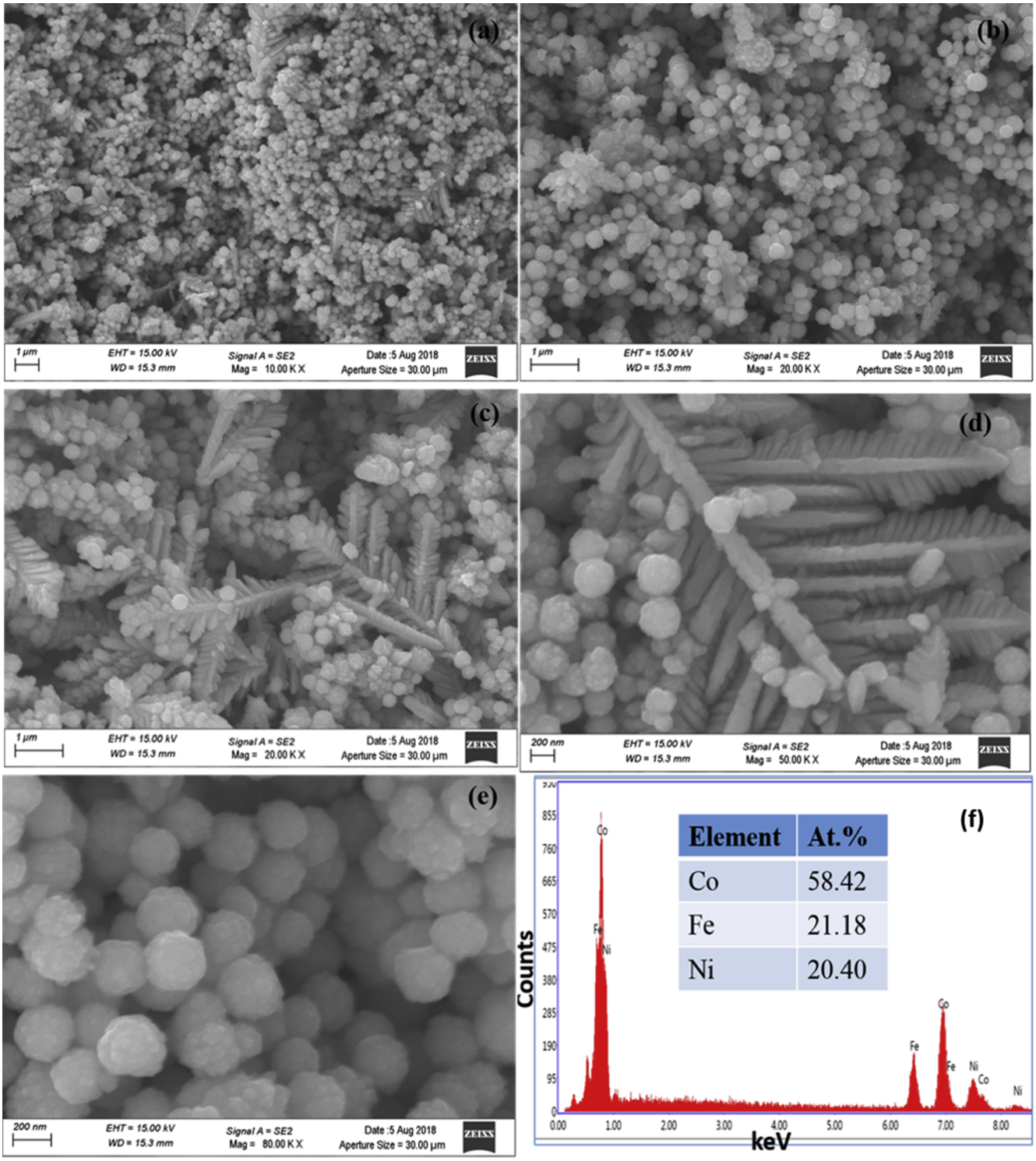

Fig. 6. (a–e) SEM images of $Co_{60}Fe_{20}Ni_{20}$ at different magnifications and (f) corresponding EDS spectrum.

($Co_{40}Fe_{40}Ni_{20}$, $Co_{50}Fe_{25}Ni_{25}$ and $Co_{60}Fe_{20}Ni_{20}$) compositions. SEM studies revealed the change in morphology with a change in the alloy composition. The phase, morphology and particle size of the synthesized alloys were found to have a significant effect on the magnetic properties of the alloys. The obtained values of saturation magnetization for Co-rich alloys synthesized through this wet chemical reduction route are found to be in the range of 111.6–138.1 emu/g with coercivity values are in the range of 101–162 Oe. In conclusion, the alloys

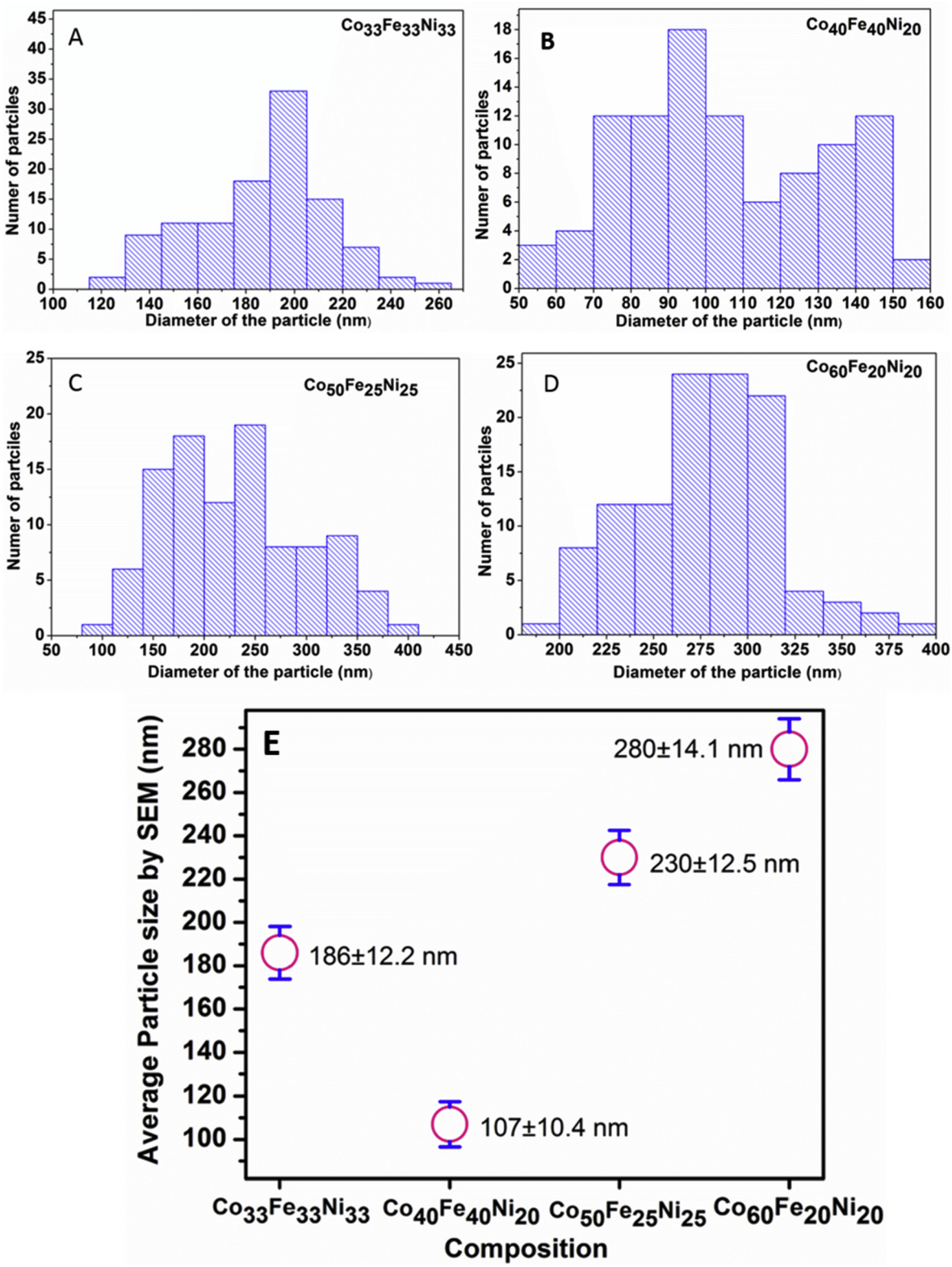

Fig. 7. (a–d) Distribution of particle size of the synthesized alloys and (e) average particle size measured from SEM images by ImageJ Software.

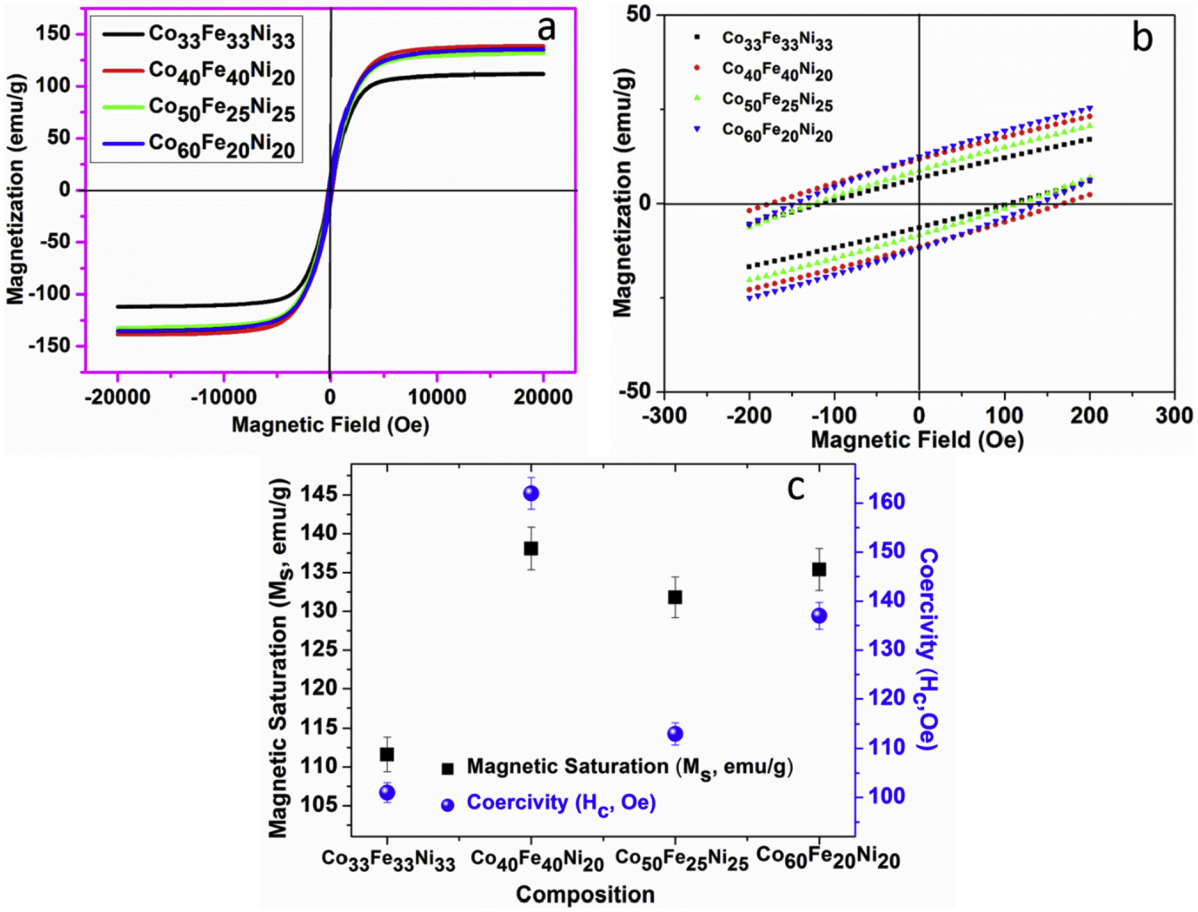

Fig. 8. (a) M-H curve of the synthesized compositions, (b) An enlarged view of the hysteresis curve at zero magnetic field and (c) Ms and Hc value for the alloys.

synthesized with this novel hydrazine reduction method possessing high saturation magnetization and coercivity can be a potential material for high-frequency magnetic applications.

Acknowledgement

We would like to thank Dr. S. Kavita from ARCI, CAEM for carrying out the magnetic characterization.

References

[1] Liu X, Gao W, Miao S, Ji B. Versatile fabrication of dendritic cobalt microstructures using CTAB in high alkali media. J Phys Chem Solids 2008;69:2665–9.
[2] Ding M, Xi J, Ji Z. Size-controlled synthesis, growth mechanism and magnetic properties of cobalt microspheres. Mater Lett 2017;201:27–30.
[3] Meng LJ, Peng XY, Zhang KW, Tang C, Zhong JX. Study structural phase transitions of FeCo and FeNi nanoparticles: a molecular dynamics study. J Appl Phys 2012;111:024303–5.
[4] Ramírez-meneses E, Torres-huerta AM, Domínguez-crespo MA. Synthesis and electrochemical characterization of Ni nanoparticles by hydrazine reduction using hydroxyethyl cellulose as capping agent, electrochim. Acta. 2014;127:228–38.
[5] Liao Q, Tannenbaum R, Wang ZL. Synthesis of $FeNi_3$ alloyed nanoparticles by hydrothermal reduction. J Phys Chem B 2006;110:14262–5.
[6] Sharifati A, Sharafi S. Structure and magnetic properties of mechanically alloyed $(Fe_{70}Co_{30})_{91}Cu_9$ powder. Mater Des 2012;36:35–40.
[7] Wu K, Wei X, Zhou X, Wu D, Liu X, Ye Y, et al. NiCo2 alloys: controllable synthesis, magnetic properties, and catalytic applications in reduction of 4-nitrophenol. J Phys Chem C 2011;115:16268–74.
[8] Osaka T. Electrodeposition of highly functional thin films for magnetic recording devices of the next century. Electrochim Acta 2000;45:3311–21.
[9] Pikula T, Oleszak D, Pękała M, Jartych E. Mössbauer study of nanocrystalline $Co_{60}Fe_{30}Ni_{10}$ and $Co_{50}Fe_{35}Ni_{15}$ alloys obtained during mechanical synthesis. J Non Cryst Solids 2008;354:4267–70.
[10] Chechenin NG, Khomenko EV, De Hosson JTM. FCC / BCC competition and enhancement of saturation magnetization in nanocrystalline Co–Ni–Fe films. JETP Lett 2007;85:212–5.
[11] Pikula T. Correlations between hyperfine magnetic field and some macroscopic magnetic quantities in mechanosynthesized CoxFeyNiz alloys. Nukleonika 2013;58:153–7.
[12] Liu X, Zangari G, Shen L. Electrodeposition of soft, high moment Co–Fe–Ni thin films. J Appl Phys 2000;87:5410–2.
[13] Pikula T, Oleszak D, Marek P, Jartych E. Structure and some magnetic properties of mechanically synthesized and thermally treated Co–Fe–Ni alloys. J Magn Magn Mater 2008;320:413–20.
[14] Baghbaderani HA, Shara S, Chermahini MD. Investigation of nanostructure formation mechanism and magnetic properties in $Fe_{45}Co_{45}Ni_{10}$ system synthesized by mechanical alloying. Powder Technol 2012;230:241–6.
[15] Kim YM, Choi D, Kim SR, Kim KH, Kim J, Han SH, et al. Magnetic properties of as-sputtered Co-Ni-Fe alloy fims. J Magn Magn Mater 2001;230:1507–9.
[16] Chechenin NG, Marchie EH, Voorthuysen V, De Hosson JTM, Boerma DO. Variation of structure and magnetic properties with thickness of thin $Co_{59}Fe_{26}Ni_{15}$ films. J Magn Magn Mater 2005;291:1539–42.
[17] Jen SU, Chiang HP, Chung CM, Kao MN. Magnetic properties of Co–Fe–Ni films. J Magn Magn Mater 2001;236:312–9.
[18] Jartych E, Żurawicz JK, Oleszak D, Pękała M. Hyperfine interactions, structure and magnetic properties of nanocrystalline Co–Fe–Ni alloys prepared by mechanical alloying. Hyperfine Interact 2006;168:989–94.
[19] Kim J, Kim J, Kim J, Kim KH, Kim J, Kim J, et al. Characterization of as-synthesized FeCo magnetic nanoparticles by coprecipitation method. J Appl Phys 2013;113:2011–4.
[20] Liu X, Zangari G, Shamsuzzoha M. Structural and magnetic characterization of electrodeposited, high moment FeCoNi films. J Electrochem Soc 2003;150:C159–68.
[21] Li X, Takahashi S. Synthesis and magnetic properties of Fe-Co-Ni nanoparticles by hydrogen plasma-etal reaction. J Magn Magn Mater 2000;214:195–203.
[22] Zhang Q, Kusada K, Wu D, Yamamoto T, Toriyama T, Matsumura S, et al. Selective control of fcc and hcp crystal structures in Au-Ru solid-solution alloy nanoparticles. Nat Commun 2018;9:510–8.
[23] Jen SU, Chiang HP, Chung CM, Kao MN. Magnetic properties of Co – Fe – Ni films. J Magn Magn Mater 2001;236:312–9.
[24] Chen H, Xu C, Zhou X, Liu Y, Zhao G. Template-free synthesis and characterization of dendritic cobalt microstructures by hydrazine reduction route. Mater Res Bull 2012;47:4353–8.
[25] Chokprasombat K, Pinitsoontorn S, Maensiri S. Effects of Ni content on nanocrystalline Fe – Co – Ni ternary alloys synthesized by a chemical reduction method. J Magn Magn Mater 2016;405:174–80.
[26] Ra MY, Pan L, Farid A. From nano-dendrite to nano-sphere of Co100-xNix alloy: composition dependent morphology, structure and magnetic properties. J Alloys Compd 2016;656:443–51.
[27] Sun Y, Liang Q, Zhang Y, Tian Y, Liu Y, Li F, et al. Controlled synthesis of magnetic Ni-Fe alloy with various morphologies by hydrothermal approach. J Magn Magn Mater 2013;332:85–8.
[28] Dalavi SB, Theerthagiri J, Raja MM, Panda RN. Synthesis, characterization and magnetic properties of nanocrystalline Fe x Ni80 – xCo20 ternary alloys. J Magn Magn Mater

2013;344:30–4.
[29] Younes A, Dilmi N, Khorchef MM, Bouamer A, Bacha N, Zergoug M. Structural and magnetic properties of FeCuNi nanostructured produced by mechanical alloying. Appl Surf Sci 2017;446:258–65.
[30] Zaharov YA, Pugachev VM, Ovcharenko VI, Datiy KA, Popova AN, Bogomyakov AS. Phase composition and magnetic properties of nanostructured Fe–Co –Ni powders. Phys Stastus Solid B. 2017;1700175:1–8.
[31] Rahsepar FR, Srivastava S, Heinig N. Shape-dependent magnetism of bimetallic FeNi nanosystems. J Mater Chem C 2014;2:6370–5.
[32] Wu H, Xu D, Wang Q, Wang Q, Su G, Wei X. Composition-controlled synthesis, structure and magnetic properties of ternary FexCoyNi100 −x−y alloys attached on carbon nanotubes. J Alloys Compd 2008;463:78–83.
[33] Chechenin NG, Khomenko EV, Vainchtein DI, De Hosson JTM, Chechenin NG, Khomenko EV, et al. Nonlinearities in composition dependence of structure parameters and magnetic properties of nanocrystalline fcc / bcc-mixed Co–Ni–Fe thin films. J Appl Phys 2008;103(103):07E738–81.
[34] Srakaew N, Jantaratana P, Nipakul P, Sirisathitkul C. Structural and magnetic properties of Fe_xNi_{100-x}alloys synthesized using Al as a reducing metal. J Magn Magn Mater 2017;435:201–5.
[35] He H-Y, Huang J-F, Fei J, Lu J, Liu T-T. Synthesis temperatture effect on the magnetic properties of $Co_{1-x}Zn_xFe_2O_4$ synthesized by a Hydrothermal Method. J Nanoelectron Optoelectron 2014;9:1–8.
[36] Hu P, Chen Z, Chang T, Deng J, Yang F. Magnetic properties of the nanoscale coral-shaped Ni-Co alloy powder with different Co contents. J Alloys Compd 2017;727:332–7.
[37] Yan Q, Li S, Pang E, Wang Y. Fabrication of hollow spheres FeCo alloy through a hydrothermal reduction method. Mater Lett 2014;120:185–8.
[38] Zhu Y, Zheng H, Yang Q, Pan A, Yang Z, Qian Y. Growth of dendritic cobalt nanocrystals at room temperature. J Cryst Growth 2004;260:427–34.
[39] Liu L, Guan J, Shi W, Sun Z, Zhao J. Facile synthesis and growth mechanism of flowerlike Ni-Fe alloy nanostructures. J Phys Chem 2010:13565–70.
[40] He HY. Structural and magnetic property of $Co_{1-x}Ni_xFe_2O_4$ nanoparticles synthesized by hydrothermal. Method 2014;636:626–36.
[41] Kr N, Vinod P. Microstructure and magnetic properties of equiatomic FeNiCo alloy synthesized by mechanical alloying. J Mater Sci: Mater Electron 2015;26:10109–18.